Superlattices and Microstructures 84 (2015) 80–90

Contents lists available at ScienceDirect

Superlattices and Microstructures

journal homepage: www.elsevier.com/locate/superlattices

Thermodynamic, structural and electronic, properties of SnO_2: By GGA and GGA + trans-blaha-modified Becke–Johnson (TB-mBJ) calculation

M.A. Bezzerrouk [a], M. Hassan [a], R. Baghdad [a,*], S. Reguieg [a], M. Bousmaha [a], B. Kharroubi [a], B. Bouhafs [b]

[a] Engineering Physics Laboratory, Faculty of Material Sciences, University Ibn Khaldoun-Tiaret, BP N°78, Zaaroura Road, 14000 Tiaret, Algeria
[b] Modeling and Simulation in Materials Science Laboratory, Physics Department, University of Sidi Bel-Abbes, Algeria

ARTICLE INFO

Article history:
Received 20 February 2015
Accepted 23 February 2015
Available online 4 May 2015

Keywords:
SnO_2
Ab initio calculations
DFT
GGA + TB-mBJ
Thermodynamic properties

ABSTRACT

In this paper we have investigated the structural, electronic and thermodynamic properties of tin oxide (SnO_2) using the full-potential linearized augmented plane wave method (FP-LAPW) within the framework of density functional theory (DFT) as implemented in the Wien2k package within the generalized gradient approximation (GGA) and GGA plus trans-blaha-modified Becke–Johnson (TB-mBJ) as the exchange correlation. From the electronic properties, SnO_2 has a direct band gap in (Γ–Γ) direction with a value of 2.86 eV. The quasi-harmonic Debye model, using a set of total energy versus volume calculations is applied to study the thermal and vibrational effects. Temperature and pressure effects on the structural parameters, such as thermal expansion, heat capacities and Debye temperature are investigated from the non-equilibrium Gibbs function.

* Corresponding author. Tel.: +213 7 99 29 94 55.
E-mail address: baghdadrachid@gmail.com (R. Baghdad).

http://dx.doi.org/10.1016/j.spmi.2015.02.046
0749-6036/

1. Introduction

Tin oxide (SnO_2) is one of the most important oxide materials; it is a n-type semiconductor, with a 3.6 eV band gap. Its rutile structure belongs to the $P4_2/mm$ space group [1]. Interestingly, the simultaneous occurrence of transparency and conductivity of SnO_2 is a unique feature among the Group-IV elements of the periodic table. Due to its excellent electrical and optical properties, SnO_2 has been used for photovoltaic devices, electrode materials, light emitting diodes, flat panel displays and gas sensors. Tin oxide attracts lots of attention because it offers many advantages: simple fabrication process, rapid response and recovery, low cost... [2,3].

First-principles electronic structure calculations of tin oxide have been reported in the literature [4–7]. Using the density functional theory (DFT) within the local-density approximation (LDA), structural, electronic and optical properties of SnO_2 have been investigated by Donglin Guo and Guo and Hu [7]. The ultraviolet absorption spectrum has been addressed by studying the optical properties [4]. Qi-Jun Liu et al. have explained the origin of the spectral peaks on the basis of the crystal-field and molecular-orbital bonding theory [8].

The behaviors of bulk SnO_2, such as phase transition, electronic properties, lattice dynamics, and optical properties have attracted sustained investigations both in experiments and theories. However, thermodynamic properties of Tin oxide have been scarce from what we have read in the literature. Thermal properties of solid are closely correlated with various fundamental physical properties, such as specific heat, melting point, inter-atomic bonding, equation of states, Debye temperature, thermal expansion coefficient. For these reasons, in the present work, *ab initio* calculations, using the full potential linearized augment plane wave method with the generalized gradient approximation (GGA) and GGA plus modified Becke and Johnson (GGA + TB-mBJ) as exchange correlation potential and quasi-harmonic Debye model, were used to investigate the structural, electronic and thermodynamic properties of Tin oxide.

2. Computational details

The first principles calculations were performed using the full potential linearized augmented plane wave (FP-LAPW) method as implemented in Wien2k code [9]. The exchange and correlation effects were treated within the generalized gradient approximation (GGA) framework [10] and generalized gradient approximation plus trans-blaha-modified Becke–Johnson (TB-mBJ) [11]. The mBJ approximation can find the band gap in better agreement with the experimental band gap. The size of basis sets was controlled by the parameter $R_{MT} \cdot K_{max}$, where R_{MT} is the smallest muffin tin radius in the unit cell and K_{max} is the magnitude of the largest K vector in reciprocal space. In our calculations we have expanded the basis function up to $R_{MT} \cdot K_{max} = 8$. The maximum value for partial waves inside atomic spheres is $l_{max} = 10$. The core energy cutoff is taken as −6.0 Ryd. The self-consistent calculations were considered to converge when the total energy difference between successive iterations is less than 10^{-5} Ry per formula unit.

The quasi-harmonic Debye model [12,13] has been applied to calculate the SnO_2 thermodynamic properties. The non-equilibrium Gibbs function $G^*(V, P, T)$ can be written as [14]:

$$G^*(V,P,T) = E(V) + PV + A_{vib}[\theta_D(V), T] \tag{1}$$

where $E(V)$ is the total energy per unit cell of SnO_2. PV *is* the constant hydrostatic pressure condition, $\theta_D(V)$ the Debye temperature and A_{vib} the vibrational Helmholtz free energy, which can be written as [15,16]:

$$A_{vib}(\theta_D, T) = nK_BT\left[\frac{9\theta_D}{8T} + 3ln\left(1 - e^{-\theta_D/T}\right) - D\left(\frac{\theta_D}{T}\right)\right] \tag{2}$$

where n is the number of atoms per formula unit, and $D\left(\frac{\theta_D}{T}\right)$ represents the Debye integral. The Debye temperature θ_D is expressed as [16]:

$$\theta_D = \frac{\hbar}{K_B}\left[6\pi^2 V^{1/2} n\right]^{1/3} f(\sigma)\sqrt{\frac{B_S}{M}} \tag{3}$$

where M is the molecular mass per unit cell and B_S is the adiabatic bulk modulus, which is approximately given by the static compressibility [13]:

$$B_S \approx B(V) = \mathrm{V}\frac{d^2E(V)}{dV^2} \tag{4}$$

$f(\sigma)$ is given by [17,18]:

$$f(\sigma) = \left\{3\left[2\left(\frac{2}{3}\frac{1+\sigma}{1-2\sigma}\right)^{3/2} + \left(\frac{1}{3}\frac{1+\sigma}{1-\sigma}\right)^{3/2}\right]^{-1}\right\}^{1/3} \tag{5}$$

where σ is Poisson ratio. Therefore, the non-equilibrium Gibbs function $G^*(V, P, T)$ can be minimized with respect to the volume V as:

$$\left[\frac{\partial G^*(V,P,T)}{\partial V}\right]_{P,T} \tag{6}$$

By solving Eq. (6), we get the thermal equation of state (EOS) $V(P, T)$.

Thermodynamic quantities such as the heat capacities C_V (at constant volume), C_p (at constant pressure), and the entropy S, have been calculated by using the following relations [14]:

$$C_V = 3nk\left[4D(\theta/T) - \frac{3\theta/T}{e^{\theta/T}-1}\right] \tag{7}$$

$$C_P = C_V(1+\alpha\gamma T) \tag{8}$$

$$S = nk\left[4D(\theta/T) - 3ln\left(1-e^{-\theta/T}\right)\right] \tag{9}$$

where α and γ are respectively the thermal expansion coefficient and the Grüneisen parameter, given by [14]

$$\alpha = \frac{\gamma C_V}{B_T V} \tag{10}$$

$$\gamma = -\frac{dln\theta(V)}{dln(V)} \tag{11}$$

The isothermal bulk modulus B_T is given by [14]

$$B_T(P,T) = V\left(\frac{\partial^2 G^*(V,P,T)}{\partial^2 V}\right)_{P,T} \tag{12}$$

SnO_2 with tetragonal rutile structure belong to the $P4_2/mnm$ space group. Experimental lattice parameters are $a_o = b = 4.737$ Å and $c = 3.186$ Å. The unit cell contains six atoms: two tin (Sn) atoms occupying the 2a Wyckoff positions, (0,0,0) and (0.5,0.5,0.5), and four oxygen (O) atoms occupying the 4f positions, $(u,u,0)$, $(-u,-u,0)$, $(0.5+u,0.5-u,0.5)$, and $(0.5-u,0.5+u,0.5)$, where $u = 0.307$ [18,19]. The electronic valence configurations for Sn and O are respectively $5s^25p^2$ and $2s^22p^4$.

3. Results and discussion

3.1. Structural properties

SnO_2 is characterized by the two lattice parameters a and c and the internal parameter u. its unit cell contains two tin atoms are set at (000; 1/21/21/2) and four oxygen atoms in the following

positions ± (u u 0; u + 1/2 1/2 − u 1/2). It is clearly seen that the oxygen atomic positions depend on the internal parameter u. The total energy is then calculated as a function of volume and the obtained data fitted to the Murnaghan equation of state [20]:

$$E(V) = \frac{B_0 V}{B_0'}\left[\frac{(V_0/V)^{B_0'}}{B_0' - 1} + 1\right] + E_0 - \frac{V_0 B_0}{B_0' - 1} \tag{13}$$

where

$$B_0 = V\frac{d^2E}{dV^2} \tag{14}$$

We have fitted the calculated E–V points to the Birch–Murnaghan equation of state (EOS) to obtain the equilibrium lattice constant a_0, bulk modulus B_0 and its pressure derivative B' [20]. The total energy as a function of volume per formula unit for SnO_2 is shown in Fig. 1. These values are listed in Table 1, together with other theoretical and experimental results. The calculated results are in good agreements with theoretical results [21–24] and experimental data [25–27]. The optimized lattice parameters a_o and c are within 0.34%, 0.35% and 0.33% from the experimental data [24–26]. The calculated bulk modulus B_o = 219.348 GPa is less than B_o = 244.7 GPa found by Bo Zhu et al. [23] and higher than B_o = 181 GPa found by Peltzer y Blancá et al. [24]. However, the calculated B_o is in good agreement when compared with experimental B_o found by Chang et al. [27]. Finally our results show that the most stable structure of the rutile-type SnO_2 occurs when a_o = 4.80 Å, c = 3.217 Å, c/a = 0.670 and u = 0.306. These values agree well with available experimental and other calculation values, indicating that the methods used in our calculations are reliable and reasonable.

3.2. Electronic properties

SnO_2 is of great interest and has found broad range of scientific and engineering applications. It has necessitated precise knowledge of the fundamental energy gap as well as the alignment of the main conduction-band valleys. The self consistent scalar relativistic band structures of SnO_2 were obtained at equilibrium volume as well as at high pressure within the GGA, and TB-mBJ schemes [11]. The band structures of SnO_2 are shown in Fig. 2. Note that the GGA method is inadequate to describe correctly the electronic properties of such materials; usually it strongly underestimates the value of the band gap energy [28,29]. The usual problem of the DFT gap underestimation encourages the researcher to find a suitable solution; TB-mBJ is a modified version of the exchange potential proposed by Becke and Johnson. This semi local exchange potential mimics very well the behavior of

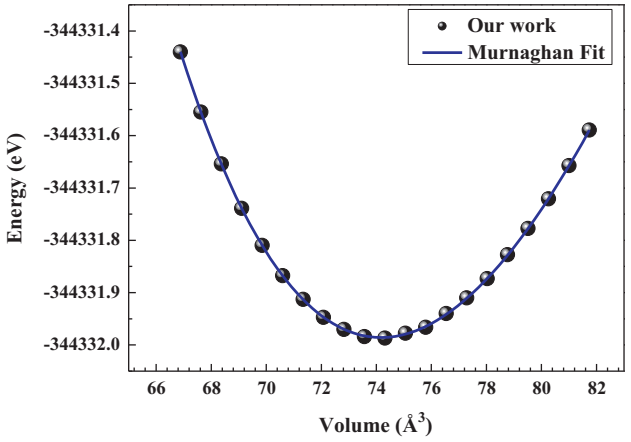

Fig. 1. Energy as a function of volume per formula unit for SnO_2.

Table 1
Our calculated (bold values), lattice parameters a_o and c, bulk modulus B_o and its pressure derivative B' of rutile-type SnO_2 at $P = 0$ GPa and $T = 0$ K, in comparison with the experimental and other theoretical data.

	a_o (Å)	c (Å)	u	B_o (GPa)	B'
Present work (GGA)	**4.80**	**3.217**	**0.3060**	**219.348**	**4.935**
GGA	4.928[a]	3.288[a]	–	204.5[a]	4.14[a]
	4.749[b]	3.142[b]	0.307[b]	–	–
Other	4.699[c]	3.165[c]	0.306[c]	244.7[c]	4.44[c]
	4.761[d]	3.184[d]	0.3061[d]	181[d]	–
Exp	4.738[e]	3.1865[e]	–	270[e]	–
	4.737[f]	3.186[f]	0.307[f]	–	–
	4.738[g]	3.186[g]	–	212[g]	5.13[g]

[a] Ref. [21].
[b] Ref. [22].
[c] Ref. [23].
[d] Ref. [24].
[e] Ref. [25].
[f] Ref. [26].
[g] Ref. [27].

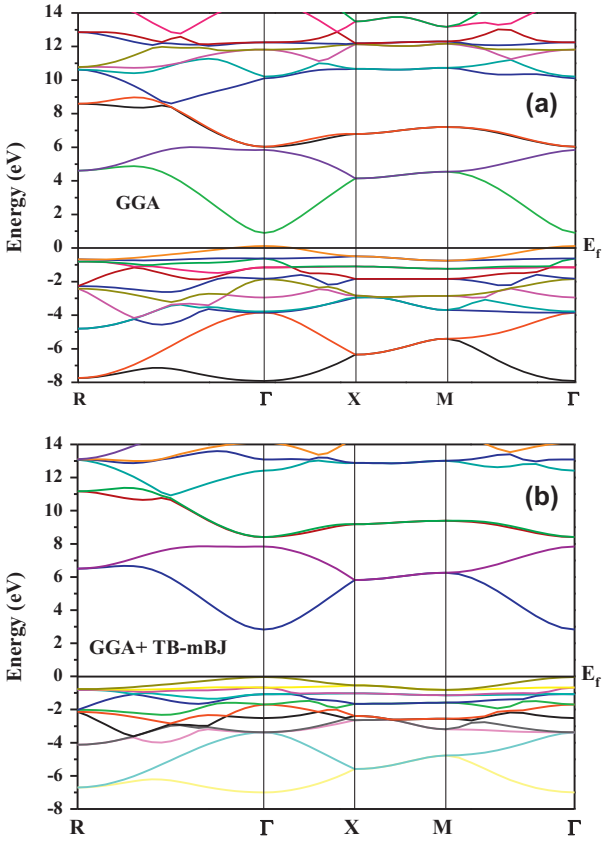

Fig. 2. Band structure of SnO_2 within GGA (a), and GGA + TB-mBJ (b).

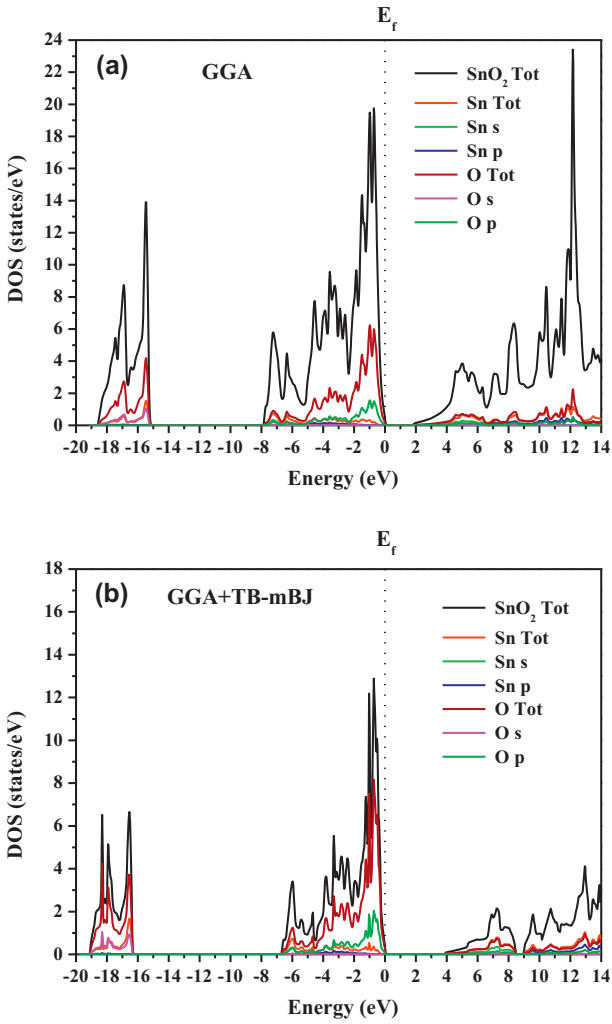

Fig. 3. Total and partial density of states of SnO_2 within GGA (a), and GGA + TB-mBJ (b).

orbital-dependent potentials and leads to calculations which are barely more expensive than GGA calculations. Therefore, it can be applied to very large systems in an efficient way.

The GGA + TB-mBJ gives a larger value of band gap than that of GGA [30]. The occupied states below the Fermi energy correspond to the valence band, whereas the unoccupied states lying above the Fermi energy correspond to the conduction band. It can be seen clearly that both conduction and valence band are located at Γ point, which means that SnO_2 has a direct band gap in Γ–Γ direction. In the direct band structure of SnO_2, the top of the valence band mostly consists of O(p) states, while the bottom of the conduction band has an anti-bonding character arising from the Sn(4s) and O(p) states. The calculate band gap by GGA is 0.77 eV, which is much smaller than the experimental 3.6 eV value [31]. In the other hand; the band gap obtained by GGA + TB-mBJ approximation is 2.86 eV, which is close to the experimental value and better than other theoretical values found in the literature: 1.38 eV by Li et al. [32], 1.08 eV by Peltzer y Blancá et al. [33], and 0.832 eV (GGA) and 2.76 eV (mBJ) by El Haj Hassan et al. [34]. The discrepancy between theoretical and experimental

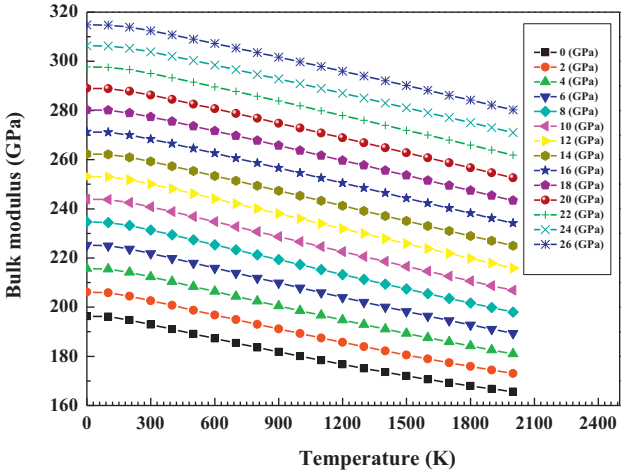

Fig. 4. Variation of the bulk modulus versus temperature at various pressures.

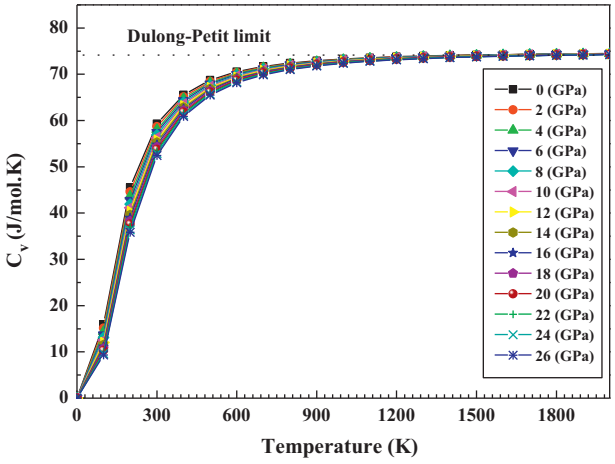

Fig. 5. Variation of the heat capacities C_V versus temperature at different pressures.

values are attributed to the fact that *ab initio* calculations performed using DFT usually underestimate the band gap [8]. Unfortunately, theoretical predictions of the band gap failed to explain the experimentally obtained band gaps.

The total and partial densities of states of SnO_2 calculated within both GGA and GGA + TB-mBJ are also shown in Fig. 3. The O-2p states are mainly predominant in the upper parts of the band structure. It is clearly seen that there is hybridization between O-2p states and Sn-5s and 5p states. We can see that the bandwidth in the lower part of the valence band is 3.62 eV and 2.95 eV and in the upper part is 8.13 eV and 6.90 eV (Respectively within GGA and GGA + TB-mBJ). Above the Fermi level, the conduction band is predominantly composed of Sn-5p and 5s states that are hybridized with O-2p. The intense peak in the conduction region take place at 12.15 eV with GGA and the most intense peak values with GGA + TB-mBJ at: (7.23, 9.58, 10.73, 12.93 eV). Our results are in good agreement with those obtained by pseudopotential GGA and FP-LAPW calculations [8,35].

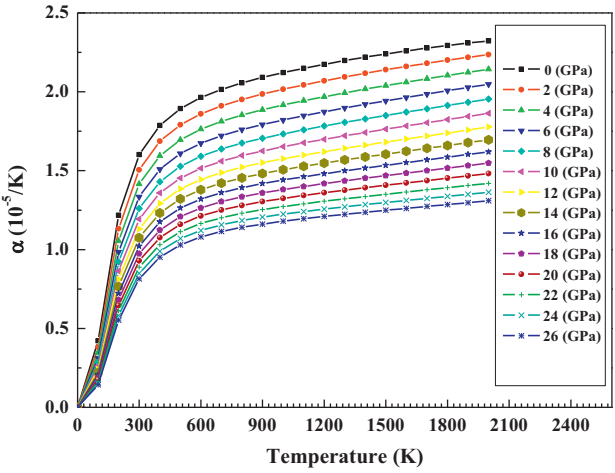

Fig. 6. Variation of the expansion coefficient versus temperature at various pressures.

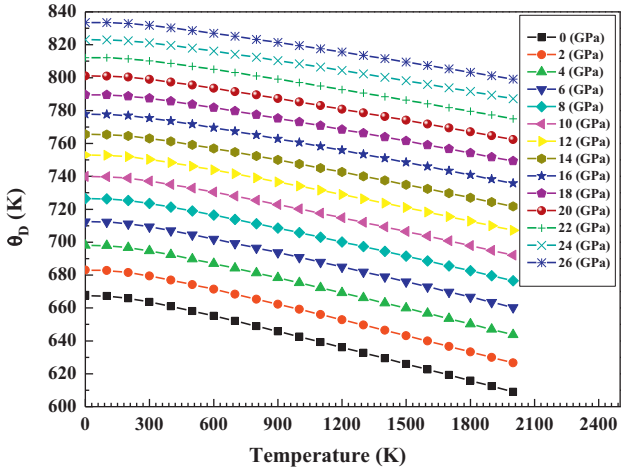

Fig. 7. Variation of Debye temperature versus temperature at various pressures.

3.3. Thermodynamic properties

Now let us discuss about the thermodynamic properties of SnO_2. These properties were determined from the calculated *E_V* data in the temperature range from 0 to 2000 K for SnO_2. This high temperature is far from the melting point. As a result the quasi-harmonic Debye model remains fully valid. The effect of pressure was studied in the range of 0–26 GPa.

First, we have studied the variation of SnO_2 bulk modulus (B_o) as a function of temperature for different values of pressure. The results are represented in Fig. 4. From this figure, we see that the bulk modulus decreases with increasing temperature at a given pressure and increases with pressure at a given temperature. The bulk modulus nearly remains constant when $T < 100$ K. Above this temperature, a linear dependence is clearly observed.

The investigation on the heat capacity of crystals is an old topic of condensed matter physics [36,37]. Two well-known limiting cases are correctly predicted by the standard elastic continuum

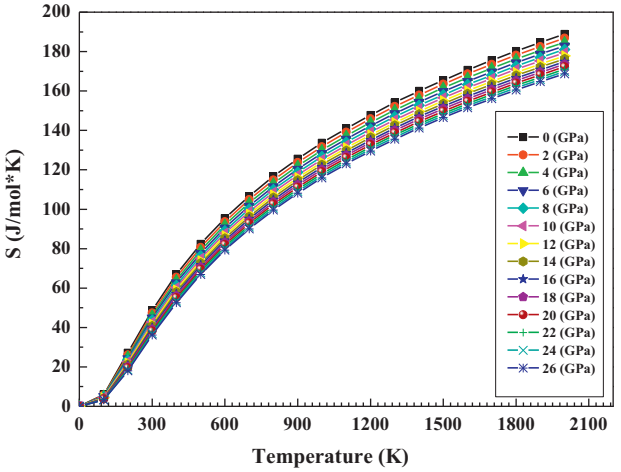

Fig. 8. Variation of the entropy versus temperature at various pressures.

Table 2
Heat capacity C_V, coefficient of thermal expansion α, debye temperature θ_D and entropy S of SnO_2 at $P = 0$ GPa and $T = 300$ K in comparison with the experimental and other theoretical data.

	C_V (J mol^{-1} K^{-1})	α (10^{-5} K^{-1})	θ_D (°K)	S (J mol^{-1} K^{-1})
Present work	**59.3**	**1.60**	**663.64**	**48.78**
Other	60[a]	3.80[a]	662[a]	52.34[d]
	74.80[e]	–	–	49.01[f]
Exp	55.84[b]	1.17[c]	–	–
	55.28[g]	–	–	51.82[g]
	53.22[h]	–	–	–

[a] Ref. [34].
[b] Ref. [39].
[c] Ref. [40].
[d] Ref. [41].
[e] Ref. [42].
[f] Ref. [43].
[g] Ref. [44].
[h] Ref. [45].

theory [37]. At high temperatures, the constant volume heat capacity (C_V) tends to the Petit and Dulong limit [38]. At sufficiently low temperatures, C_V is proportional to T^3 [38]. We present in Fig. 5. the temperature dependence of the isochoric (C_V) heat capacity for SnO_2. $C_V(T)$ indicates a sharp increase up to ~800 K, which is attributed to the anharmonic approximation of the Debye model used here. However, at high temperature, the constant volume heat capacity C_V tends to the Dulong-Petit limit, which is common for all solids. At room temperature we find that C_V is about 59.3 J mol^{-1} K^{-1} which is in good agreement with the experimental value of Cp in the rutile-type (55.84 J mol^{-1} K^{-1} [34]). Our result is closer to the experimental values than the value of 74.80 J mol^{-1} K^{-1} reported by Miiller et al. [42].

The fractional increase in length per unit rise in temperature is called the material's coefficient of thermal expansion. This is an important physical property of the materials. The calculated thermal expansion coefficient of SnO_2 as a function of temperature and pressure is shown in Fig. 6. Our calculated value of 1.60×10^{-5} K^{-1} is in a better concordance with the experimental value of 1.17×10^{-5} K^{-1} reported by P.S. Peercy and Morosin [43] than the theoretical value of 3.80×10^{-5} K^{-1} found in Ref. [34]. It is shown that the thermal expansion coefficient α also rapidly

increases with T up to 500 K and then linearly increases for higher temperatures. The increase of α with T becomes smaller as pressure increases. The thermal expansion coefficient α gets very small for higher temperatures and higher pressures.

The Debye temperature θ_D is a very important parameter, which is related to many physical properties of solids, such as specific heat and melting temperature. Fig. 7. displaying the variation of the Debye temperature θ_D with respect to the temperature clearly shows that θ_D is nearly constant from 0 to 120 K and decreases linearly with increasing temperature from $T > 120$ K. At zero pressure and 300 K, the obtained Debye temperature values for SnO_2 is about 663.64 K, which is in good agreement with the nearly 662 K value computed by El Haj Hassan et al. [34].

Finally, we finish our work with the calculation of entropy (S), which is related to the notions of order and disorder. It also gives useful information that is required to specify the exact physical state of a system, given its thermodynamic specification**.** Our calculated value of 48.78 J/mol K, which concords with the experimental value of 51.82 J/mol K given by Gurevich et al. [40] and theoretical value of 52.34 J/mol K given by Ref. [44] and 49.01 J/mol K given by Ref. [45]. The calculated entropy for SnO_2 under various pressures as a function of temperature is presented in Fig. 8. It is confirmed that the entropy increases exponentially with the rising of temperature. At the same time it decreases with increasing pressure.

Heat capacity C_V, coefficient of thermal expansion α, Debye temperature θ_D and entropy S of SnO_2 have been calculated for $P = 0$ GPa and $T = 300$ K. Results are gathered in Table 2, where experimental values and other theoretical results are recalled for sake of comparison.

4. Conclusion

In summary, we have performed detailed *ab initio* calculations within the generalized gradient approximation (GGA) and GGA plus modified Becke and Johnson (TB-mBJ) as exchange correlation potential, to study the structural, electronic and thermodynamic properties of SnO_2. The structural results such as the lattice parameters and bulk modulus are in good agreement with the previous theoretical and experimental data. Our calculated electronic properties show that SnO_2 has direct band gap with a value of 2.86 eV, which is found closer to the experimental value and to be in very good agreement with theoretical data available. Thermodynamic quantities such as the heat capacity, the thermal expansion coefficient, the Debye temperature and the entropy, have been calculated using the quasi-harmonic Debye model for various values of temperature and pressure. Hence, this study can light the way for more investigation of this popular oxide material for various chemical and physical applications.

Acknowledgements

Authors would like to thank Dr. Lisa Michez from the CINaM, UPR3118 CNRS, Campus de Luminy case 913, 13288 Marseille cedex 9, France; for many helpful discussions.

References

[1] PCPDFWIN, JCPDS 88–0287, International Center for Diffraction Data, 2002.
[2] T. Suzuki, T. Yanazaki, H. Yoshioka, M. Hikichi, J. Mater. Sci. 23 (1988) 1106–1111.
[3] S.R. Wang, Y.Q. Zhao, J. Huang, Y. Wang, H.X. Ren, S.H. Wu, S.M. Zhao, W.P. Huan, Appl. Surf. Sci. 253 (2007) 3057–3061.
[4] Ph. Barbarat, S.F. Matar, Comput. Mater. Sci. 10 (1998) 368.
[5] Y.W. Li, Y. Li, T. Cui, L.J. Zhang, Y.M. Ma, G.T. Zou, J. Phys, Condens. Matter. 19 (2007) 425230.
[6] S.F. Matar, D. Jung, M.A. Subramanian, Solid State Commun. 152 (2012) 349–353.
[7] Donglin Guo, Hu Chenguo, Appl. Surf. Sci. 258 (2012) 6987–6992.
[8] Qi-Jun Liu, Zheng-Tang Liu, Li-Ping Feng, Comput. Mater. Sci. 47 (2010) 1016–1022.
[9] P. Blaha, K. Schwarz, G. Madsen, D. Kvasnicka, J. Liutz, in: K. Schwarz (Ed.), Wien2k, An Augmented Plane Wave Plus Local Orbitals Program for Calculating Crystal Properties, Techn. University, Wien, Austria, 2001.
[10] J.P. Perdew, Y. Wang, M. Ernzerhof, Phys. Rev. Lett. 77 (1996) 3865–3868.
[11] F. Tran, P. Blaha, Phys. Rev. Lett. 102 (2009) 226401.
[12] H.J. Monkhorst, J.D. Pack, Phys. Rev. B 13 (1976) 5188–5192.
[13] F. Peng, H.Z. Fu, X.D. Yang, Physica B 403 (2008) 2851–2855.
[14] M.A. Blanco, E. Francisco, V. Luaña, Comput. Phys. Commun. 158 (2004) 57–72.

[15] M.A. Blanco, A.M. Pendás, E. Francisco, J.M. Recio, R. Franco, J. Mol. Struct. Theochem. 368 (1996) 245–255.
[16] M. Flórez, J.M. Recio, E. Francisco, M.A. Blanco, A.M. Pendás, Phys. Rev. B 66 (2002) 144112.
[17] E. Francisco, J.M. Recio, M.A. Blanco, A. Martín Pendás, J. Phys. Chem. 102 (1998) 1595–1601.
[18] E. Francisco, M.A. Blanco, G. Sanjurjo, Phys. Rev. B 63 (2001) 094107.
[19] K. Ellmer, J. Phys. D 34 (2001) 3097–3108.
[20] F.D. Murnaghan, Proc. Natl. Acad. Sci. U.S.A. 30 (1944) 244–247.
[21] Chun.-Mei. Liu, Xiang.-Rong. Chen, Guang.-Fu. Ji, Comput. Mater. Sci. 50 (2011) 1571–1577.
[22] Z. Zhu, R.C. Deka, A. Chutia, R. Sahnoun, H. Tsuboi, M. Koyama, N. Hatakeyama, A. Endou, H. Takaba, C.A. Del Caprio, M. Kubo, A. Miyamoto, Phys. Chem. Solids 70 (2009) 1248–1255.
[23] Bo Zhu, Chun-Mei Liu, Ming-Bang Lv, Xiang-Rong Chen, Jun Zhu, Guang-Fu Ji, Phys. B 406 (2011) 3508–3513.
[24] E.L. Peltzer y Blancá, A. Svane, N.E. Christensen, Phys. Rev. B 48 (1993) 15712–15718.
[25] J.Z. Jiang, L. Gerward, J.S. Olsen, Scripta Mater. 44 (2001) 1983–1986.
[26] R. Wyckoff, Crystal Structures, 2nd ed., Wiley Interscience, New York, 1964.
[27] E. Chang, E.K. Graham, J. Geophys. Res. 80 (1975) 2595–2599.
[28] P. Dufek, P. Blaha, K. Schwarz, Phys. Rev. B 50 (1994). 7279-7238.
[29] S. Fahy, K.J. Chang, S.G. Louis, M.L. Cohen, Phys. Rev. B 35 (1989) 7840–7847.
[30] B. Ealet, M.H. Elyakhloufi, E. Gillet, M. Ricci, Thin Solid Films 250 (1994) 92–100.
[31] V.T. Agekyan, Phys. Status Solidi A 43 (1977) 11–42.
[32] Y. Li, W. Fan, H. Sun, X. Cheng, P. Li, X. Zhao, J. Hao, M. Jiang, J. Phys. Chem. A 114 (2010) 1052.
[33] E.L. Peltzer y Blancá, A. Svane, N.E. Christensen, C.O. Rodríguez, O.M. Cappannini, M.S. Moreno, Phys. Rev. B 48 (1993) 15712–15718.
[34] F. El Haj Hassan, S. Moussawi, W. Noun, C. Salameh, A.V. Postnikov, Comput. Mater. Sci 72 (2013) 86–92.
[35] Leonardo.A. Errico, Physica B 389 (2007) 140–144.
[36] A. Einstein, Ann. Phys. 22 (1907) 180–190.
[37] P. Debye, Ann. Phys. 39 (1912) 789–839.
[38] A.T. Petit, P.L. Dulong, Ann. Chim. Phys. 10 (1819) 395–413.
[39] V.B. Polyakov, S.D. Mineev, R.N. Clayton, G. Hu, V.M. Gurevich, D.A. Khramov, K.S. Gavrichev, V.E. Gorbunov, L.N. Golushina, Geochim. Cosmochim. Acta 69 (2005) 1287–1300.
[40] V.M. Gurevich, K.S. Gavrich, V.E. Gorbunov, B.B. Polyakov, S.D. Mineev, L.N. Golushina, Geohimiâ 10 (2004) 1096–1105.
[41] D.Y. Zhogin, E.A. Kosarukina, V.P. Kolesov, Zh. Fiz. Khim. 54 (1980) 916–920.
[42] Wojciech Miiller, Gordon J. Kearley, Chris D. Ling, Theor. Chem. Acc. 131 (2012) 1216–1223.
[43] P.S. Peercy, B. Morosin, Phys. Rev. B 7 (1973) 2779–2786.
[44] D'Ans-Lax: Taschenbuch f. Chemiker u. Physiker, vol. 1, Springer, Berlin, Heidelberg, New York, 1967.
[45] R.H. Lamoreaux, D.L. Hildenbrand, L. Brewer, J. Phys. Chem. 16 (1987) 419–443.